

Electronic Supporting Information

Tandem electrocatalytic CO₂ reduction with Fe-porphyrins and Cu-nanocubes enhances ethylene production

Min Wang, ^{[a]†} Vasilis Nikolaou, ^{[b]†} Anna Loiudice, ^[a,c] Ian D. Sharp, ^[c] Antoni Llobet, ^{[b,d]*}
Raffaella Buonsanti ^{[a]*}

^a*Laboratory of Nanochemistry for Energy (LNCE), Institute of Chemical Sciences and Engineering (ISIC), École Polytechnique Fédérale de Lausanne, CH-1950 Sion, Switzerland.*

^b*Institute of Chemical Research of Catalonia (ICIQ), Barcelona Institute of Science and Technology (BIST), 43007, Tarragona, Spain.*

^c*Walter Schottky Institute and Physics Department, Technische Universität München, Am Coulombwall 4, 85748 Garching, Germany.*

^d*Departament de Química, Universitat Autònoma de Barcelona (UAB), Cerdanyola del Vallès, 08193 Barcelona, Spain.*

*Correspondence to: allobet@iciq.cat, raffaella.buonsanti@epfl.ch

† These authors have equally contributed.

Content

Experimental Section	3
Chemicals.....	3
Synthesis of Cu _{cub}	4
Electrochemical electrodes preparation process	4
Materials characterization	5
Electrochemical Measurements	6
Results Section	10
Synthetic approach for Fe-TbcTPP and Fe-TBTPP.....	10
Synthesis of H ₂ TbcTPP.....	10
Synthesis of Fe-TbcTPP	11
Synthesis of Fe-TBTPP.....	12
Fig. S1. ¹ H NMR of H ₂ TbcTPP.	13
Fig. S2. ¹³ C NMR of H ₂ TbcTPP.	13
Fig. S3. MALDI-TOF of Fe-TbcTPP.	14
Fig. S4. MALDI-TOF of Fe-TBTPP	14
Table S1. Key electrochemical and spectroscopic data for the Fe-Pors	15
Fig. S5. FEs and current density of the Fe-Pors.....	16
Fig. S6. (a) TEM image and (b) XRD of the as-synthesized Cu _{cub}	16
Fig. S7. Cu _{cub} /Fe-Por CO ₂ RR performance at -0.45 and -0.55V vs RHE.....	17
Fig. S8. Cu _{cub} /Fe-TBTPP CO ₂ RR performance at -1.15 V vs RHE.....	17
Fig. S9. Cu _{sph} /Fe-TBTPP CO ₂ RR performance at -1.05 V vs RHE	18
Fig. S10. CVs used to determine the capacitance and the electrochemically active surface areas ...	19
Fig. S11. (a) FE _{C1 (CH₄+HCOO⁻)} and (b) partial current density for the C _{1 (CH₄+HCOO⁻)} products	20
Fig. S12. XPS spectra of the Cu 2 <i>p</i> and Cu LMM regions of Cu _{cub} and Cu _{cub} /Fe-Por.	20
Fig. S13. (a) FEs and (b) partial current density for the CO product.....	21
Fig. S14. <i>j</i> _{total} vs. scan-rate to determine the sample capacitance.....	22
Fig. S15. Cu _{cub} /Fe-TBTPP CO ₂ RR performance with different loading of Cu _{cub}	22
Fig. S16. FT-IR of the Cu _{cub} before and after ligand stripping	23
Fig. S17. UV-vis after 1.5 h electrolysis at -1.05 V vs RHE	24
Fig. S18. TEM images after 1.5 h electrolysis at -1.05 V vs RHE	24
Fig. S19. Stability study of Cu _{cub} /Fe-TBTPP at -1.05 V vs RHE	25
References	25

Experimental Section

Chemicals. All chemicals were used as received, with no further purification. Tri-n-octylphosphine oxide (TOPO, 99%), Copper(I) bromide (CuBr, 99.999%), Oleylamine (OLAM, 70%), Tetrahydrofuran (THF), Hexane, Toluene (anhydrous, 99.8%) and Nafion® perfluorinated resin solution (5wt. % in lower aliphatic alcohols and water, contains 15-20% water) was purchased from Sigma-Aldrich. K₂CO₃ (99+ %) was purchased from Acros.

Synthesis of Cu cubes. Cu cubes were synthesized following the procedure introduced in our previous work.¹ TOPO (24 mmol, 9.37 g) was first mixed with OLAM (117ml) in a three-necked 250 ml flask equipped with reflux condenser and internal thermocouple temperature controller and degassed under vacuum with vigorous magnetic stirring at room temperature. After the gas evolution was no longer observed, CuBr (5 mmol, 0.71 g) was quickly added to the solution under nitrogen flow. Then the resulting solution was rapidly heated to 260 °C and held at reflux at this temperature for 1 h before being cooled down to room temperature naturally. The solution was then transferred into a glove box, where it was divided into six centrifuge tubes. Hexane (22.5 ml) was added to each tube and then centrifuged at 6000 rpm for 10 min. The precipitate was recovered in a minimal amount of hexane, an equal amount of ethanol was added, and then the resulting solution was centrifuged for an additional 10 min at 6000 rpm. The precipitate was finally recovered with toluene and stored in a glove box. The Cu concentration of the Cu cube stock solution was measured by ICP-OES, as described below. Typically, a Cu cube stock solution with a concentration of 0.06 mM was obtained.

Before the electrochemical testing, it is necessary to remove the native ligands to avoid possible interference with the catalytic activity. A mild-solvent washing method is effective to remove the binding organic ligands off the surface. After such washing in acetone 3 successive times, most of the ligands were removed, which was confirmed by FT-IR (**Fig. S16a**).

Electrochemical electrodes preparation process.

Fe-Por stock solution. The Fe-TBTPP, Fe-TPP and Fe-TbcTPP were separately dissolved in THF and used as the stock solution at a concentration of 1 mg/mL.

Fe-Por/CNTs. Multiwalled carbon nanotubes (3mg of CNTs) were dispersed in THF (3 mL) by sonication. The desired stock solution of Fe-TBTPP (318 μ L), Fe-TPP (246 μ L) or Fe-TbcTPP (360 μ L) was then added to the suspension, followed by sonication. Then, after the addition of a small amount of Nafion® perfluorinated resin solution (5wt. % in lower aliphatic alcohols and water, contains 15-20% water) (15 μ L), the ink of Fe-TBTPP/CNTs (260 μ L), Fe-TPP/CNTs (240 μ L) or Fe-TbcTPP/CNTs (266 μ L) was drop casted onto a glassy carbon electrode for electrolysis. The loading of the molecular catalysts was 16 nmol/cm² for all CO₂RR experiments reported in Fig. 3.

Cu_{cub}/Fe-Por tandem catalyst.

Cu_{cub}/Fe-Por electrodes with a Fe-Por electrode surface concentration of 8 nmol/cm² were prepared as follows: the desired stock solution of Fe-TBTPP (9.6 μ L), Fe-TPP (7.5 μ L) or Fe-TbcTPP (10.8 μ L) was added to the Cu_{cub} in THF (26.6 μ g / 7 μ L) with sonication to achieve thorough mixing. The resulting solution was finally drop casted on a glassy carbon electrode for subsequent CO₂RR experiments. The Cu_{cub}/Fe-Por at different loading reported in Fig. 6 were prepared by adjusting the amount of added stock solution of the molecular catalysts.

We note that the addition of CNTs in the Cu_{cub}/Fe-Por ink was intentionally avoided. A dedicated study is ongoing to understand the transfer mechanism of CO to the surface of Cu, which can occur via direct spillover or diffusion in the electrolyte followed by adsorption on the Cu surface. Initial results suggest that the CNTs play a role. Thus, minimizing the number of components in the tandem catalysts aided the interpretation of the results reported in this manuscript.

Materials characterization.

Nuclear Magnetic Resonance (NMR) spectroscopy: A Bruker Avance 400 MHz spectrometer was used to perform the NMR characterization. Two-dimensional NMR experiments (COSY, HSQC and HMBC) were also performed in order to assign all ^1H and ^{13}C NMR signals. All measurements were carried out at room temperature in a deuterated solvent using residual protons as internal reference.

Ultraviolet–visible (UV-vis) absorption spectroscopy: A Cary 50 (Varian) UV-Vis spectrophotometer was used for all absorption studies. The reported experiments were performed using a standard 1 cm pathway UV-Vis cuvette.

Mass spectrometry: A BRUKER Autoflex Matrix Assisted Laser Desorption Ionization (MALDI) time-of-flight mass spectrometer was employed for recording MALDI-TOF mass spectra. Samples were dissolved in the appropriate solvent and mixed with a matrix when necessary.

Transmission electron microscopy (TEM): TEM images were acquired on a FEI Tecnai-Spirit at 120 kV. Nanocrystals were drop-casted on a copper TEM grid (Ted Pella, Inc.) prior to imaging.

X-ray Diffraction (XRD): The XRD patterns were acquired on a Bruker D8 Advance diffractometer with a $\text{Cu K}\alpha$ source equipped with a Lynxeye one-dimensional detector. Samples were prepared by drop-casting nanoparticles on the clean conductive silicon wafers.

Inductively Coupled Plasma Optical Emission Spectrometry (ICP-OES): ICP-OES was performed on an Agilent 5100 spectrometer to determine the solution concentration of synthesized Cu cubes. The sample solution was prepared by overnight digestion in 70% ICP grade HNO_3 followed by opportune dilution with DI water to obtain the 2% acid content needed for the analysis.

X-Ray photoelectron spectroscopy (XPS): XPS was performed using an Axis Supra (Kratos Analytical) instrument, using the monochromated $K\alpha$ X-ray line of an Al anode. The pass energy was set to 20 eV with a step size of 0.1 eV. The samples were prepared by drop-casting films onto clean conductive silicon wafers. The binding energy scale was referenced to 284.5 eV using the C-C component of the C 1s core level.

Fourier transform infra-red spectroscopy (FT-IR): FT-IR was carried out on a Perkin Elmer Two spectrometer using an attenuated total reflectance (ATR) plate. Air was used as a background spectrum. Samples were prepared by drop-casting THF suspensions of the Cu_{cub} and $Cu_{cub}/Fe-Por$ directly onto the ATR plate and leaving it to air-dry. Spectra were recorded with a resolution of 4 cm^{-1} and a total of 16 scans.

Electrochemical Measurements.

Homogeneous. All the homogeneous cyclic voltammetry (CV) measurements were performed with a CHI660D potentiostat using a one-compartment three-electrode cell. A glassy carbon disk (GC_d , $\varnothing = 0.3\text{ cm}$, $S = 0.07\text{ cm}^2$) was employed as working electrode (WE), a platinum (Pt) disk ($\varnothing = 0.2\text{ cm}$, $S = 0.03\text{ cm}^2$) as counter electrode (CE) and $Ag/AgNO_3$ (0.01 M $AgNO_3$, 0.1 M tetrabutylammonium hexafluorophosphate ($TBAPF_6$) in acetonitrile) was used as reference electrode (RE). Before each experiment, the working electrodes were polished with alumina powder (granulometry $0.5\text{ }\mu\text{m}$), washed with distilled water and sonicated in acetone for 5 min. Dry and degassed dimethylformamide (DMF) solution was employed for all electrochemical measurements, to which the necessary amount of $TBAPF_6$ was added as supporting electrolyte to yield a 0.1 M ionic strength. CVs were recorded at a scan rate of 100 mV/s. All the reported potentials in this work were converted to NHE by adding 0.609 V to the measured potential using the ferrocene (Fc)/ferrocenium (Fc^+) redox couple as internal standard for correction.²⁻³

Heterogeneous. The electrochemical CO₂ reduction reaction experiments were performed using a Biologic SP-300 potentiostat in a polycarbonate electrochemical cell (H-cell). Typically, working electrodes (cathode electrodes) were prepared by drop-casting the freshly prepared ink within a circular area of 1.33 cm² on glassy carbon plates (2.5 cm × 2.5 cm, Type 2, Alfa Aesar). Platinum foil and an Ag/AgCl electrode (leak free series, Innovative Instruments, Inc.) were used as the counter electrode and reference electrode, respectively. A Selemion anion exchange membrane was used to separate the anodic and cathodic compartments. Before loading electrocatalysts, glassy carbon supports were typically polished using a 1 μm diamond, followed by rinsing with Milli-Q water and ultrasonication in acetone for 5 min twice. Then, aqueous KHCO₃ (0.1 M) was used as the electrolyte (2 mL in each half of the cell). During electrolysis, CO₂ was constantly bubbled through the electrolyte at a flow rate of 5 sccm, which was controlled by a mass flow controller (Bronkhorst), and the gas was first humidified with water by passing it through a bubbler to minimize evaporation of electrolyte. The gas was vented from the anode compartment to the atmosphere, whilst the gas from the cathode compartment was fed directly to an in-line gas chromatograph for analysis. For the analysis of gaseous products, a gas chromatograph (GC, SRI instruments) equipped with a HayeSep D porous polymer column, thermal conductivity detector, and flame ionization detector was used. Ultra-high purity N₂ (99.999%) was used as a carrier gas. The concentration of gaseous products was determined using calibration curves from standard gas mixtures. For liquid product analysis, high-performance liquid chromatography (HPLC) was carried out on an UltiMate 3000 instrument from Thermo Scientific. 5 mM H₂SO was used as the eluent for the HPLC measurements.

Voltages were converted to the RHE scale by using a calibrated reference electrode according to the equation below. At 298 K, the $E_{\frac{Ag}{AgCl}}$ is the working potential.

$$E_{RHE} = E_{\frac{Ag}{AgCl}} + 0.0591 \times pH + E_{\frac{Ag}{AgCl}}^{\circ}$$

$$E_{\frac{Ag}{AgCl}}^{\circ} = 0.206V$$

Manual ohmic drop correction was applied with every chronoamperometry experiment according to the following equation

$$E_{\frac{Ag}{AgCl-applied}} = E_{\frac{Ag}{AgCl}} + (i \times R)$$

where i is the measured current and R is the ohmic drop across the cell determined by electrochemical impedance spectroscopy (EIS).

The **turnover frequency for CO (TOF_{CO})** is the turnover number (TON) of CO per unit time.

$$TON = \frac{n_{CO}}{n_{cat}}$$

$$TOF = \frac{TON}{t}$$

n_{CO} are the moles of CO, n_{cat} are the total moles of catalyst deposited on the electrode, t is the time of the chronoamperometry experiment. The assumption that all Fe-Por on the electrode are active provides an underestimation of the TOF.

Electrochemical impedance spectroscopy (EIS) was used to determine the electrochemical cell resistance (R_{cell}) and the charge-transfer resistance (RCT). Four spectra were measured at the open-circuit potential, using 41 points between 1 MHz and 100 Hz, using a sinusoid amplitude of 20 mV and a pause time of 0.6 s between each frequency. The value for resistance compensation was taken either from the Nyquist plot (taking the value of $Re(Z)$ at the minimum value of $-Im(Z)$ before the charge-transfer arc), or from the plot of $|Z|$ against frequency, using the asymptotic value of $|Z|$.

Electrochemically active surface area (ECSA) and current normalization analysis relies on the Electrochemical Double Layer (ECDL) capacitance of the electrode in this work. Cyclic voltammograms (CVs) were first recorded between 0.2 V and 0.25 V vs. RHE (in a region where non-faradaic process takes place) at incremented scan-rates between 4 and 32 mV s⁻¹. The current density difference between the cathodic (j_c) and anodic (j_a) sweeps at a given voltage scales linearly with the scan rate (v), and the slope of the line is equal to the double-layer capacitance C_{DL} :

$$C_{DL} = \frac{j_c - j_a}{v}$$

Using the same method to find the capacitance of a bare glassy carbon electrode as reference, we calculate the surface roughness factor (SRF).

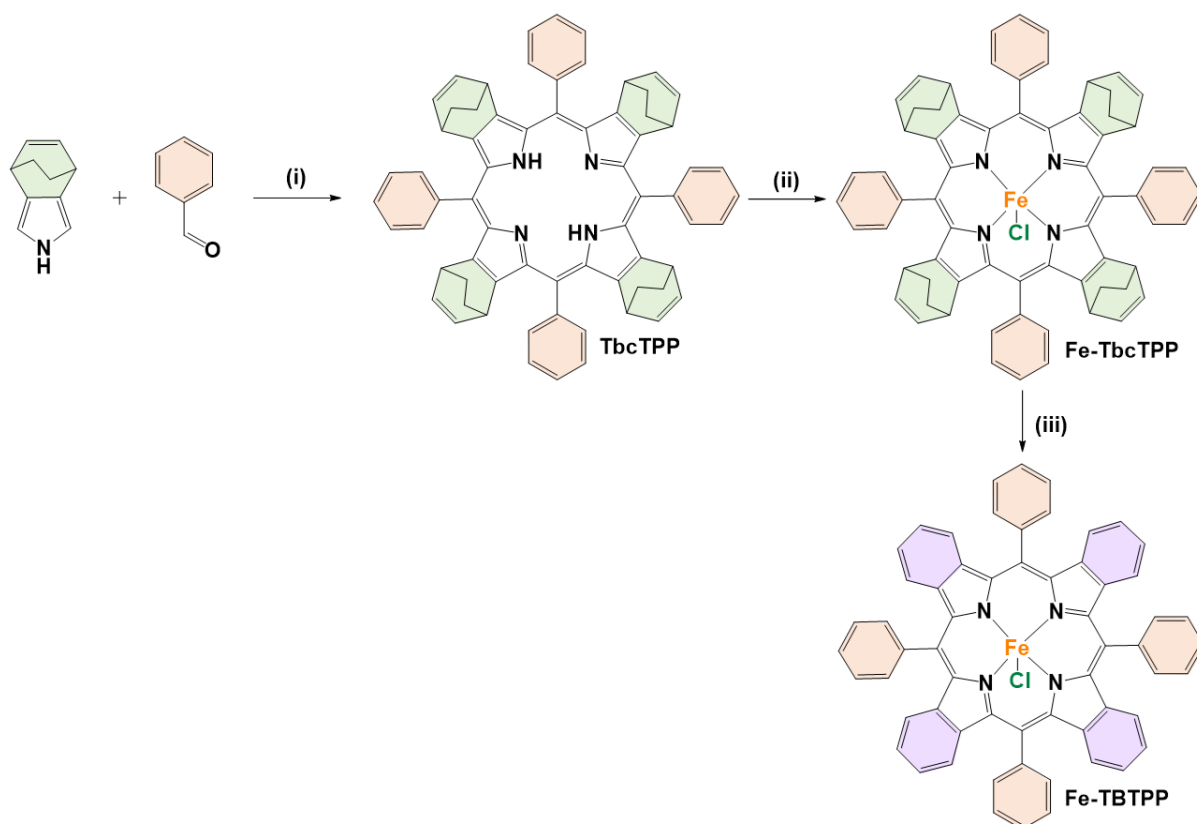
$$SRF = \frac{C_{DL} (sample)}{C_{DL} (reference)}$$

Finally, the Normalisation Factor (NF) is calculated using the geometric area of the electrode exposed to the electrolyte.

$$NF = SRF \times Geometric Area$$

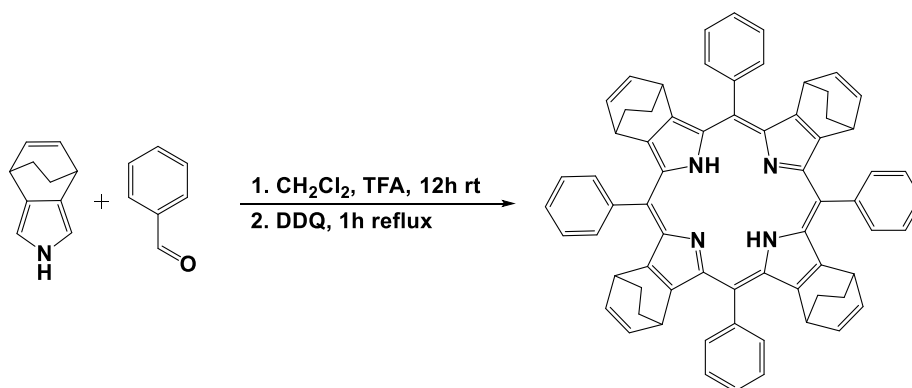
Results Section

Synthetic approach for Fe-TbcTPP and Fe-TBTTP.



Scheme S1. Schematic drawing of the synthetic approach followed for the preparation of **Fe-TbcTPP** and **Fe-TBTTP**. i) CH_2Cl_2 , TFA, DDQ, 12h, ii) FeBr_2 , 2,6-lutidine, THF, 66 °C, 12 h; iii) vacuum, 200°C, 1h.

Synthesis of tetrabicyclo[2.2.2]octadiene-tetraphenyl porphyrin (H_2TbcTPP)



In a two neck round bottom flask, 4,7-dihydro-4,7-ethano-2H-isoindole (0.2 g, 1.4×10^{-3} mol, bc-pyrrole)^[4] and benzaldehyde (0.15g, 1.4×10^{-3} mol) were dissolved in 140 mL of CH_2Cl_2 . The solution was covered with aluminum foil and bubbled with N_2 for 15 min. Subsequently, TFA (0.024 mL, 1.4×10^{-4} mol) was added and the reaction mixture was stirred overnight (12 h) at room temperature (rt). Then, 2,3-Dichloro-5,6-dicyano-1,4-benzoquinone (DDQ) 0.32 g, 1.4×10^{-3} mol) was added and the mixture was stirred under reflux for 1 h. Upon the completion of the reaction, a short filtration was performed using a column containing silica gel and CH_2Cl_2 as eluent.

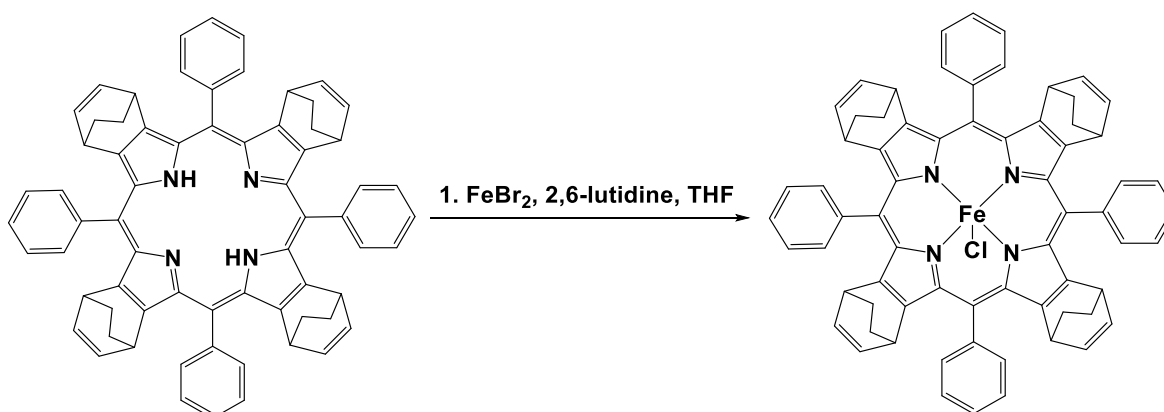
To purify tetrabicyclo[2.2.2]octadiene-tetraphenyl porphyrin (**H₂TbcTPP**), column chromatography was performed using $\text{CH}_2\text{Cl}_2/\text{MeOH}$ (99:1) as a solvent mixture to obtain **H₂TbcTPP** as a pure product, yield: 20% (0.064 g, 7×10^{-5} mol).

¹H NMR (400 MHz, CDCl₃): δ = 8.34 (m, 8H), 7.86 (m, 12H), 6.46 (m, 8H), 3.41 (m, 8H), 1.37 (m, 16H), -3.42 (s, 2H) ppm.

¹³C NMR (100 MHz, CDCl₃): δ = 143.3, 136.6, 135.4, 135.3, 135.1, 128.3, 127.0, 117.4, 37.4 and 27.0 ppm.

UV/Vis (THF): λ_{max} [$\log(\epsilon/M^{-1}\text{cm}^{-1})$] = 426 (5.25), 521 (4.18), 557 (3.54), 598 (3.61), 662 (3.06) nm.

Synthesis of iron(III)-chlorido-tetrabicyclo[2.2.2]octadiene-tetraphenyl porphyrin (Fe-TbcTPP).



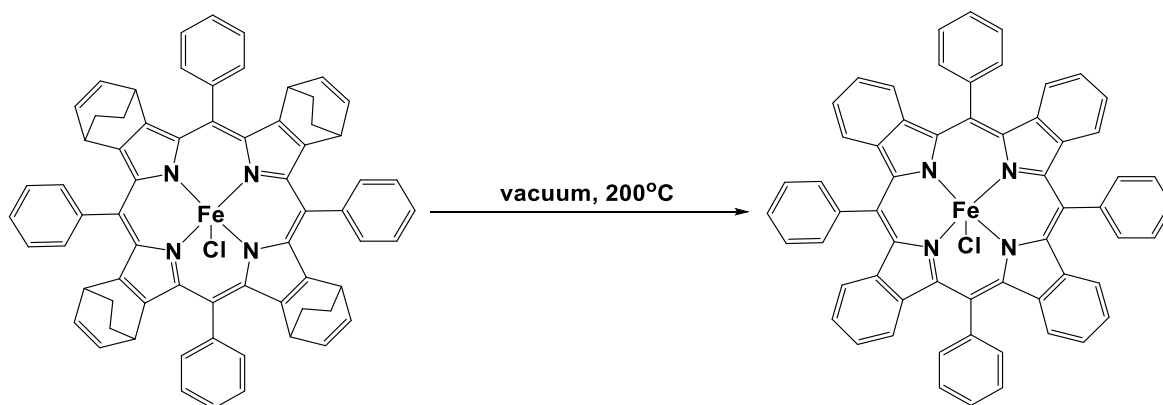
A two-neck Schlenk round bottom flask was first loaded with **H₂TbcTPP** (0.050 g, 5.4×10^{-5} mol). Then, anhydrous FeBr₂ (0.15 g, 8×10^{-4} mol) was added to the Schlenk flask. Outside of the glove box, dry THF (20 mL) and 2,6-lutidine (0.028 mL, 2.7×10^{-4} mol) were added under Ar and the reaction mixture was stirred at 66 °C for 12 h. The solvent was removed under reduced pressure and the resulting solid was solubilized in DCM and washed with brine, HCl (solution of 1M) and dried over Na₂SO₄. The crude product was purified by silica gel column chromatography using DCM as eluent and a layer of NaCl on the top of the silica, yielding 0.048 g (88%) of **Fe-TbcTPP**.

Fe-TbcTPP:

MS (MALDI-TOF): m/z calc. for [M] C₆₈H₅₂ClFeN₄: 1015.3237, found: 1015.3230.

UV/Vis (THF): λ_{max} [$\log(\epsilon/M^{-1}cm^{-1})$] = 392 (4.85), 424 (4.77), 514 (3.90) nm.

Synthesis of iron(III)-chlorido-tetrabenzotetraphenyl porphyrin (Fe-TBTPP).



In a round bottom schlenk flask, **Fe-TbcTPP** (0.045 g, 4.4×10^{-5} mol) was heated to 200 °C under reduced pressure for 1 h. Then, silica gel column chromatography was performed using DCM as eluent and a layer of NaCl on the top of the silica, yielding 0.038 g (95%) of **Fe-TBTPP**.

MS (MALDI-TOF): m/z calc. for [M] C₆₀H₃₆ClFeN₄: 903.1978, found: 903.1952.

UV/Vis (THF): λ_{max} [$\log(\epsilon/M^{-1}cm^{-1})$] = 429 (4.85), 451 (4.89), 561 (4.25), 603 (4.32), 641 (4.16), 756 (3.81) nm.

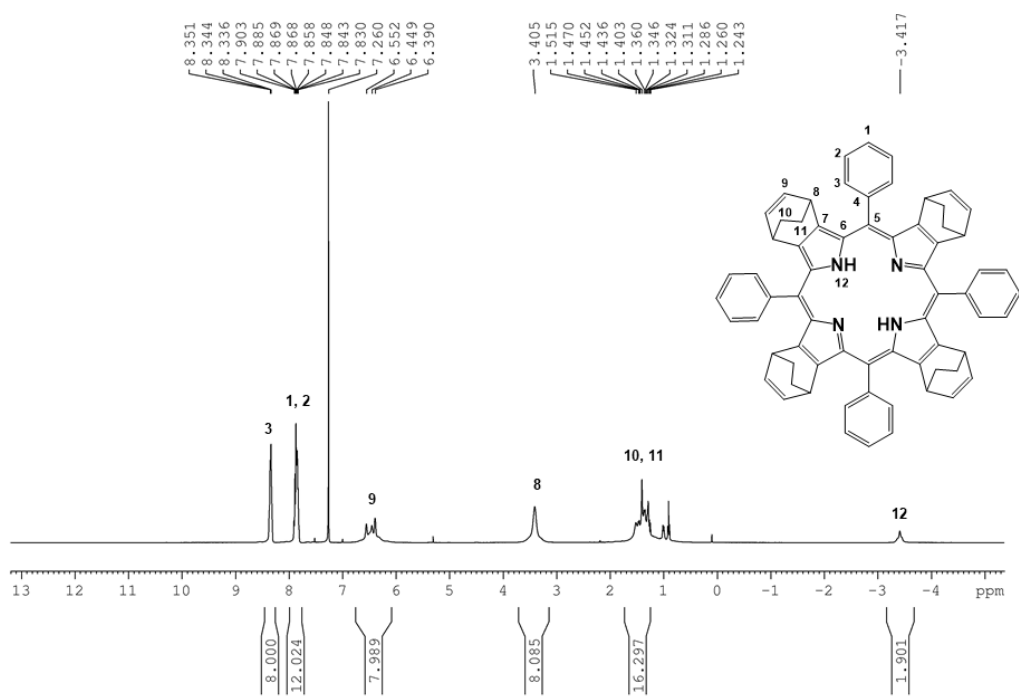


Fig. S1. ^1H NMR of H_2TbcTPP (400MHz, CDCl_3).

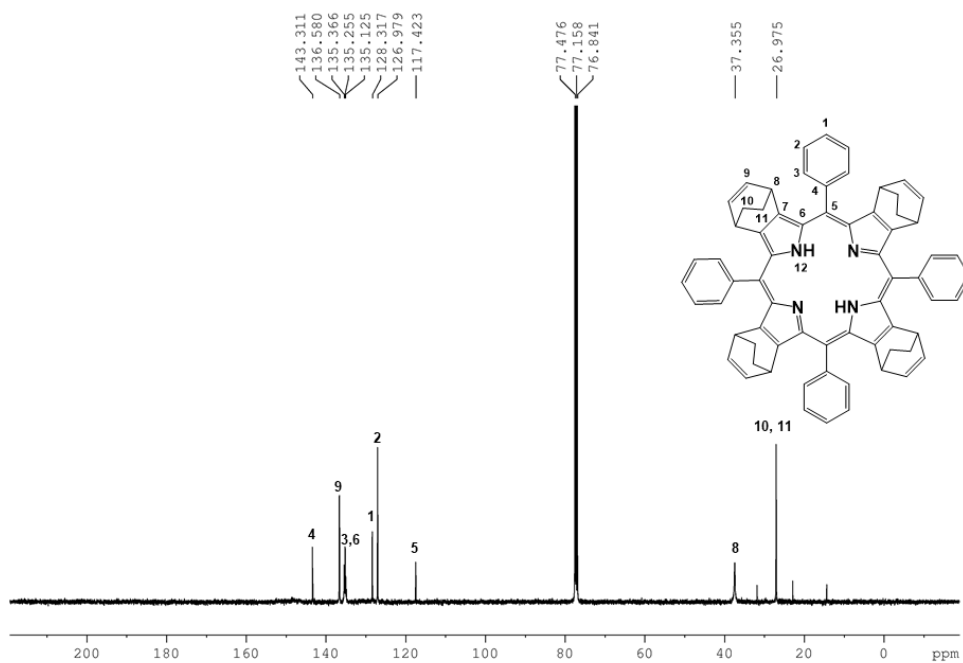


Fig. S2. ^{13}C NMR of H_2TbcTPP (100MHz, CDCl_3).

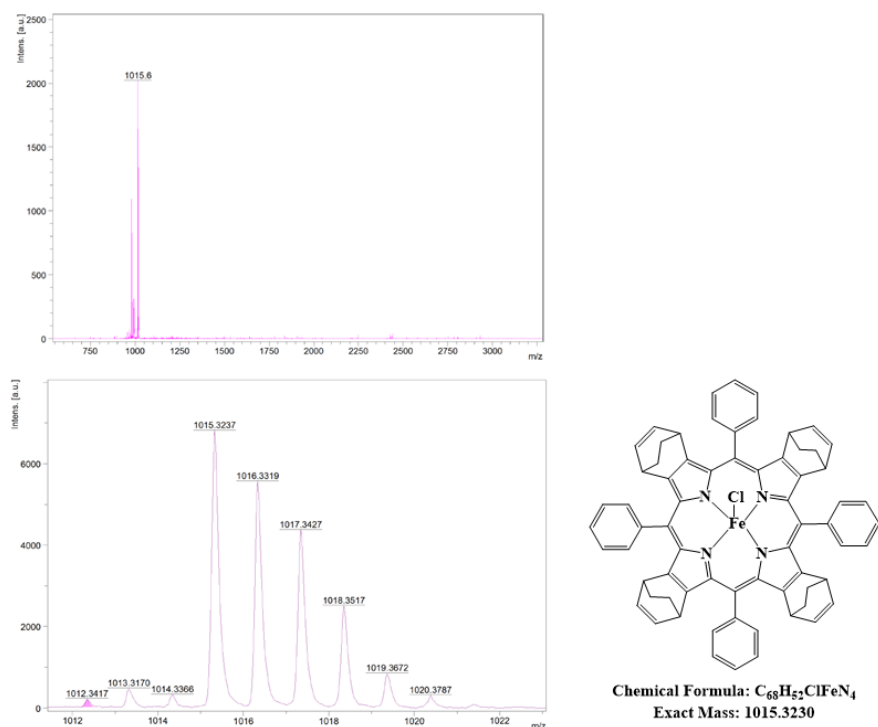


Fig. S3. MALDI-TOF nominal and accurate mass spectra of **Fe-TbcTPP**.

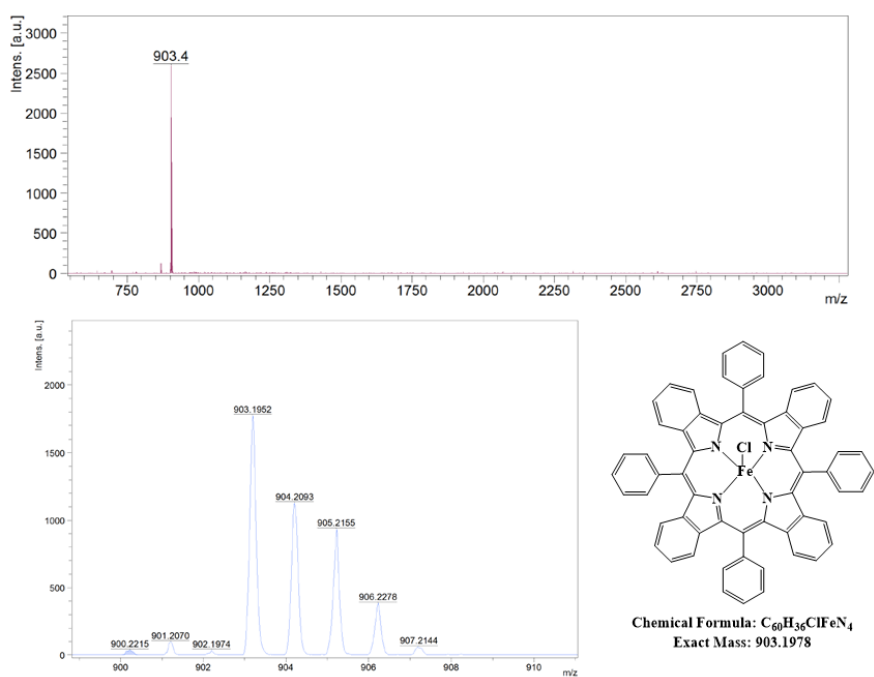


Fig. S4. MALDI-TOF nominal and accurate mass spectra of **Fe-TBTPP**.

Table S1. Key electrochemical and spectroscopic data for the **Fe-Pors** discussed in this work.^a

Porphyrin	E° (V) ^b			λ_{max} Soret band (nm)
	Fe ^{III/II}	Fe ^{III/I}	Fe ^{I/0}	[log ϵ (M ⁻¹ cm ⁻¹)]
Fe-TBTPP	0.16	-0.76	-1.36	451 [4.89]
Fe-TPP	0.07	-0.81	-1.44	417 [4.99]
Fe-TbcTPP	-0.10	-1.00	-1.65	392 [4.85]

^a see text for experimental details,

^b E° reported vs. NHE.

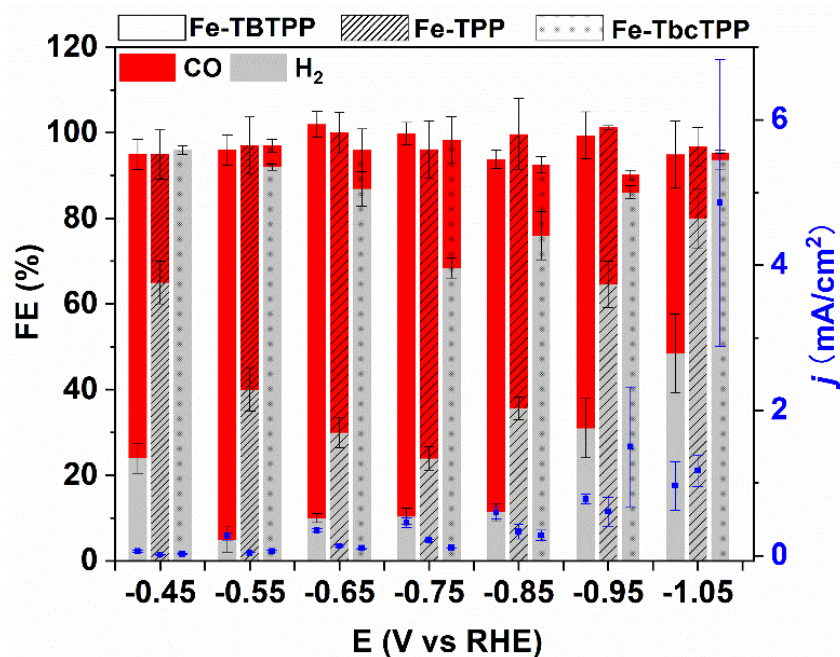


Fig. S5. FEs and current density of the Fe-Por molecules measured at a loading of 16 nmol/cm² on carbon nanotubes in a H-cell with CO₂ saturated 0.1M KHCO₃ electrolyte. The reported values are averages of three independent experiments with the error bars indicating the standard deviation.

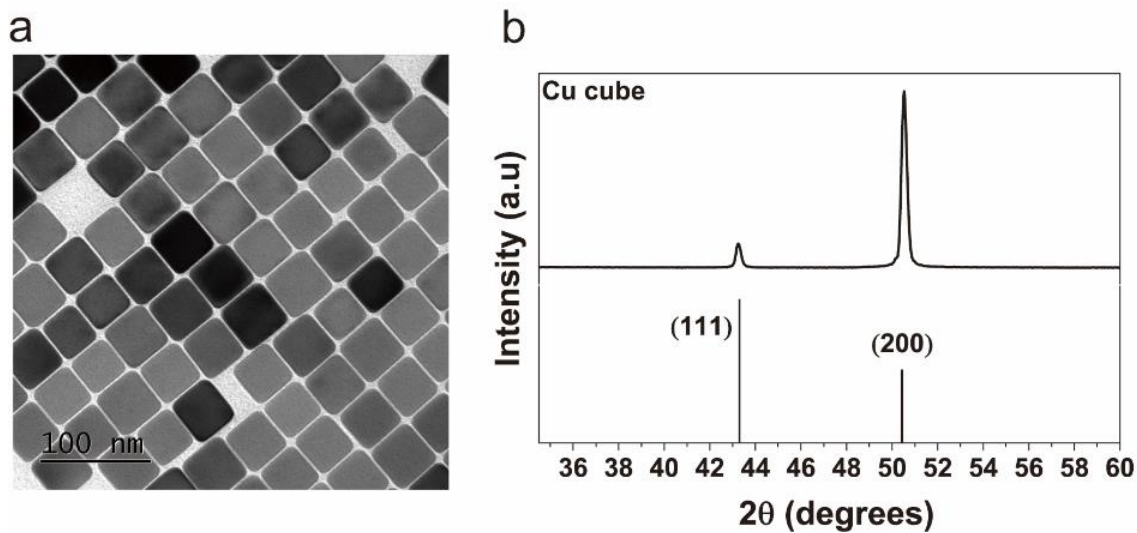


Fig. S6. (a) TEM image and (b) XRD of the as-synthesized Cu cubes.

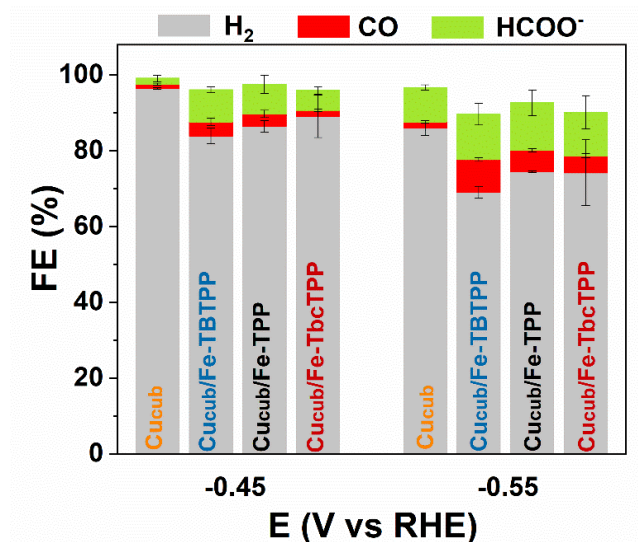


Fig. S7. CO₂RR performance in the H-cell system with CO₂ saturated aqueous 0.1 M KHCO₃ as electrolyte. Total FEs over Cu_{cub}, Cu_{cub}/Fe-TPP, Cu_{cub}/Fe-TBTPP and Cu_{cub}/Fe-TbcTPP at -0.45 V and -0.55 V vs RHE, prior to the observed onset of appreciable C-C coupling. The reported values are averages of two independent experiments.

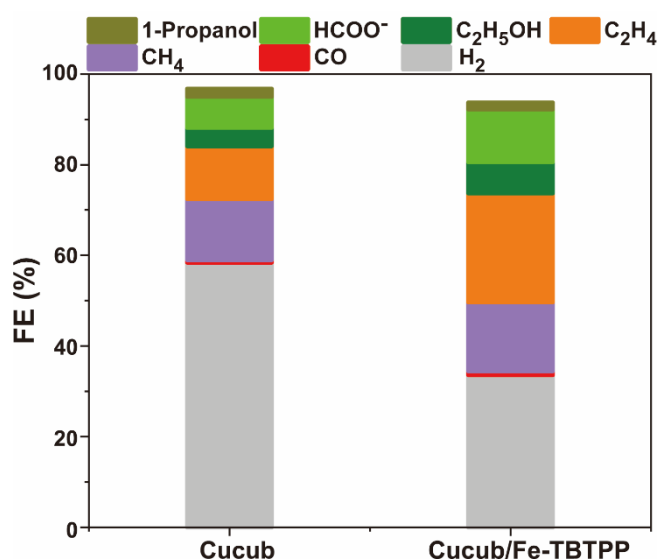


Fig. S8. Total FEs for Cu_{cub} and Cu_{cub}/Fe-TBTPP at -1.15 V vs RHE with CO₂ saturated aqueous 0.1 M KHCO₃ as the electrolyte.

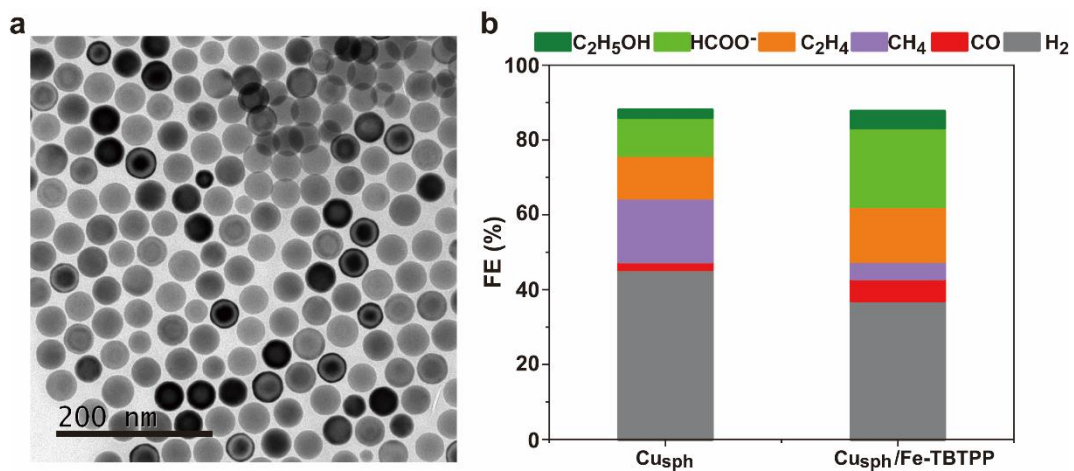


Figure S9. (a) TEM image of the as-synthesized Cu spheres (Cu_{sph}) and (b) FEs for Cu_{sph} and Cu_{sph}/ Fe-TBTPP with the loading of Fe-TBTPP and of Cu_{sph} being 8 nmol/cm² and 3.12 x 10² nmol/cm², respectively, at -1.05 V vs RHE in the CO₂ saturated 0.1 M KHCO₃ H-cell.

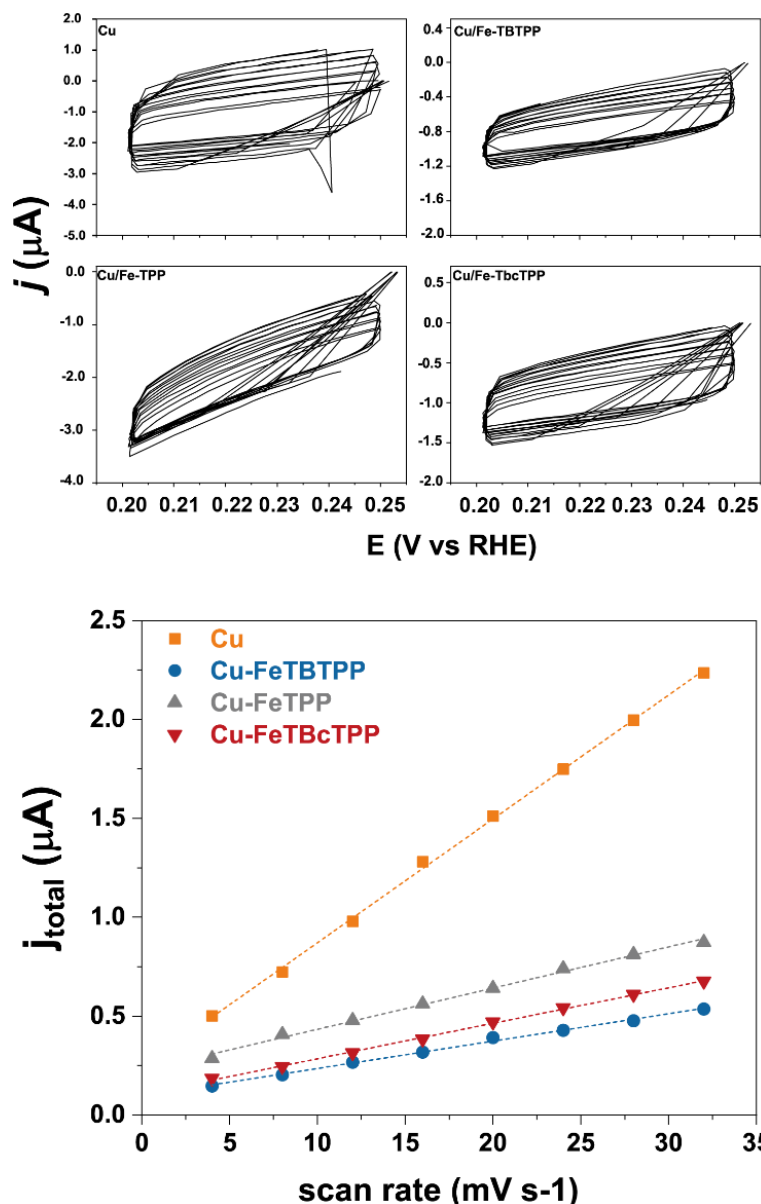


Fig. S10. Representative examples of cyclic voltammograms used to determine the capacitance and the electrochemically active surface areas for Cu_{cub} and $\text{Cu}_{\text{cub}}/\text{Fe-Por}$ samples. j_{total} ($j_{\text{total}} = j_{\text{c}} - j_{\text{a}}$ values were taken to calculate j_{total} at 0.215 V vs RHE) plotted against the scan-rate to determine the sample capacitance.

As described above, we chose the capacitance of the clean and blank glassy carbon ($S_{\text{geom}} = 1.33 \text{ cm}^2$) as a reference capacitance value to determine the SRF ($C_{\text{ref}} = 23.4 \mu\text{F}/\text{cm}^2$). The ratio of C_{sample} by C_{ref} gives a surface roughness factor (SRF). Then, the Normalization Factor (NF) for $20 \mu\text{g}/\text{cm}^2$ of Cu_{cub} was 2.82 cm^2 , and that for $\text{Cu}_{\text{cub}}/\text{Fe-TPP}$, $\text{Cu}_{\text{cub}}/\text{Fe-TBTPP}$ and $\text{Cu}_{\text{cub}}/\text{Fe-TbcTPP}$ ($3.12 \times 10^2 \text{ nmol}/\text{cm}^2$ of Cu_{cub} and $8 \text{ nmol}/\text{cm}^2$ of the Fe-Por) were found to be 1.20,

0.91 and 0.96 cm^2 , respectively. Finally, with the NF value, all the currents can be modified to give current density values from the electrochemically active surface area (ECSA).

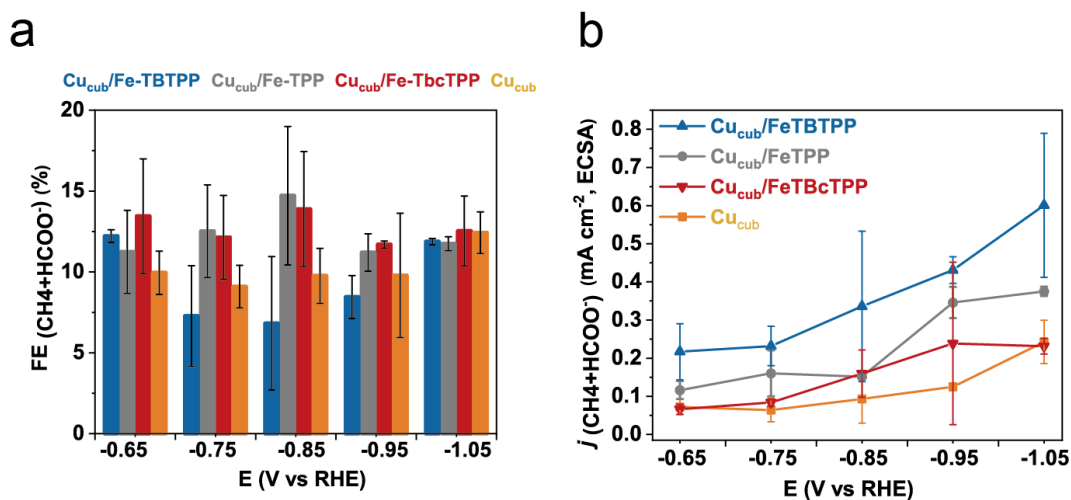


Fig. S11. (a) $\text{FE}_{\text{C}_1(\text{CH}_4+\text{HCOO}^-)}$ and (b) partial current density for the $\text{C}_1(\text{CH}_4+\text{HCOO}^-)$ products ($j_{\text{CH}_4+\text{HCOO}^-}$) normalized by ECSA of Cu_{cub} , $\text{Cu}_{\text{cub}}/\text{Fe-TPP}$, $\text{Cu}_{\text{cub}}/\text{Fe-TBTPP}$ and $\text{Cu}_{\text{cub}}/\text{Fe-TbcTPP}$ at different potentials. The reported values are an average of three independent experiments with error bars indicating the standard deviations.

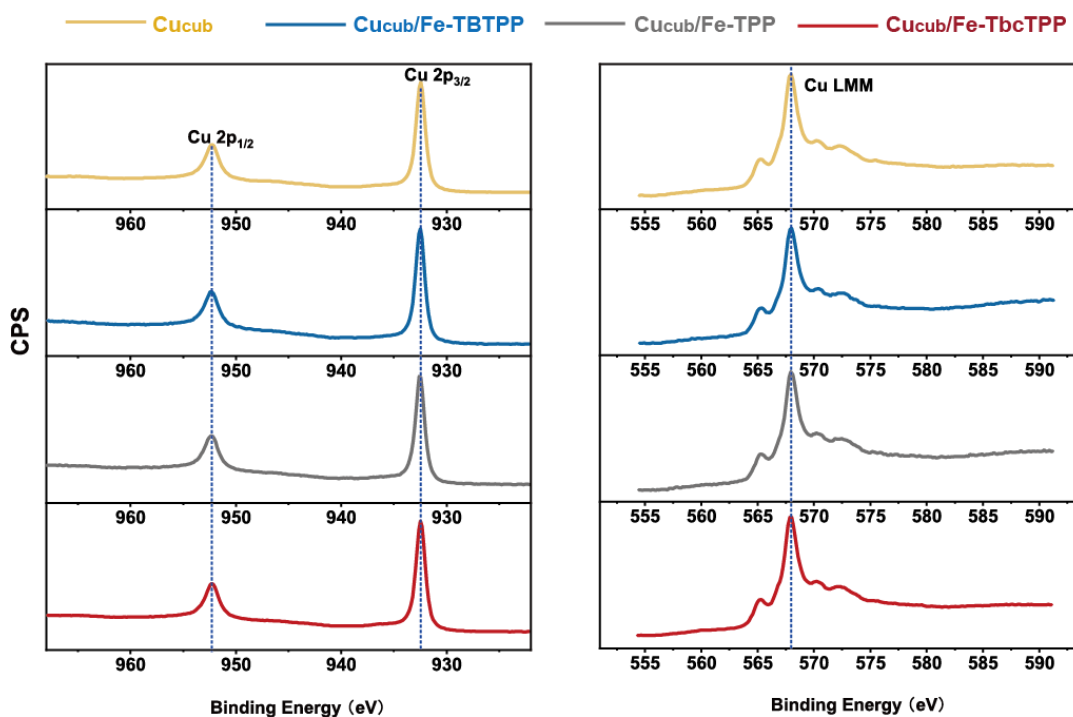


Fig. S12. XPS spectra of the $\text{Cu } 2p$ and Cu LMM regions of Cu_{cub} and $\text{Cu}_{\text{cub}}/\text{Fe-Por}$.

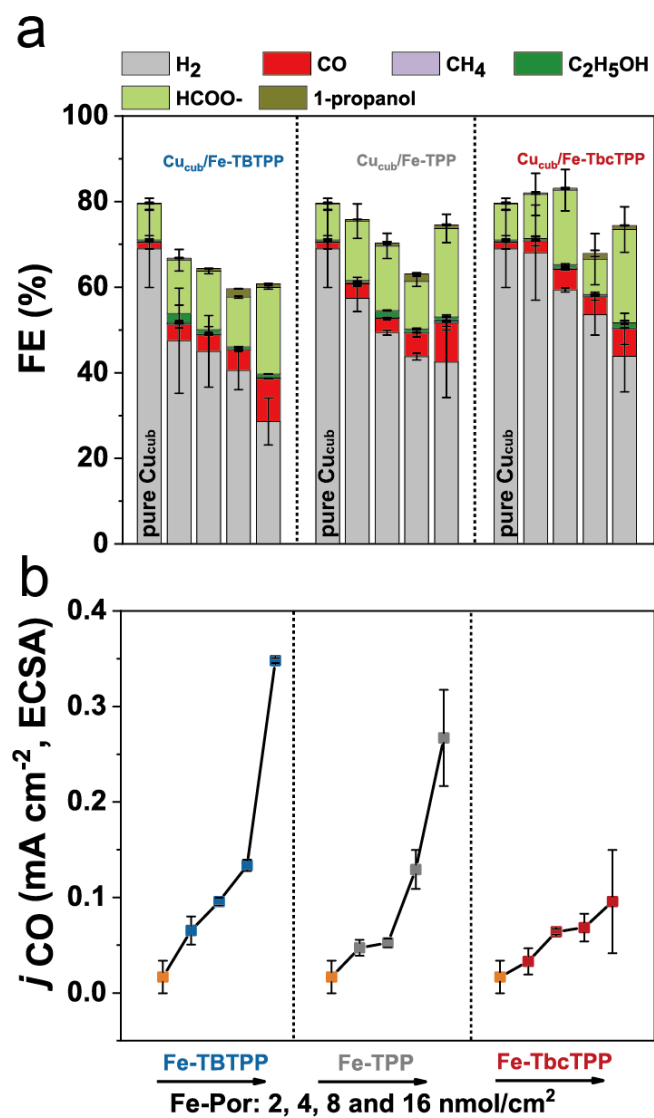


Fig. S13. (a) FEs and (b) partial current density for the CO product normalized by ECSA ($j_{CO}/ECSA$) for different loading of Fe-Por (2, 4, 8 or 16 nmol/cm²) at a constant Cu_{cub} loading (3.12×10^2 nmol/cm²) at -0.95 V vs RHE in the CO₂ saturated 0.1 M KHCO₃ H-cell. The error bars represent the standard deviations from measurements of three independent electrodes.

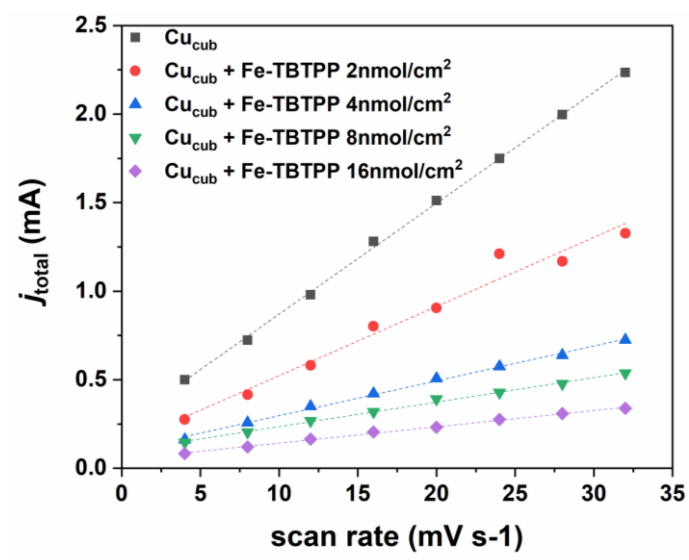


Fig. S14. j_{total} at 0.215 V vs RHE plotted against the scan-rate to determine the sample capacitance for Cu_{cub} /Fe-TBTPP samples with different molecule loadings (2, 4, 8 or 16 nmol/cm^2) and constant Cu_{cub} loading ($3.12 \times 10^2 \text{ nmol}/\text{cm}^2$).

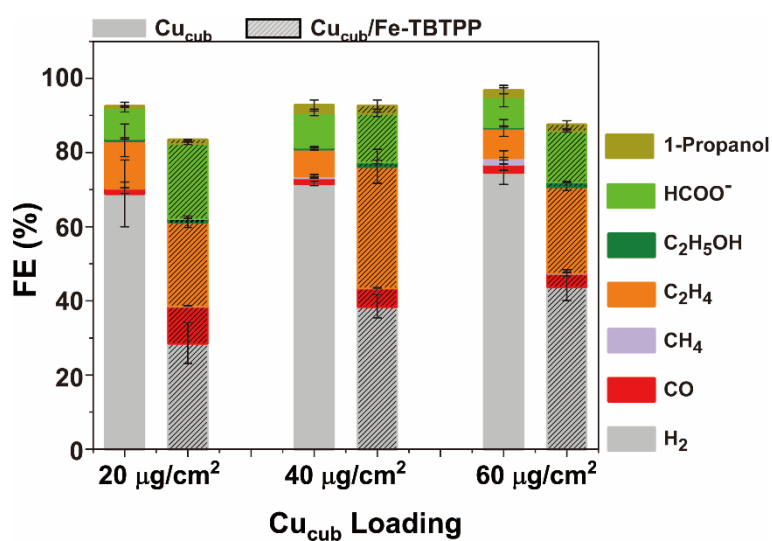


Fig. S15. Total FEs for different loading of Cu_{cub} (3.12×10^2 , 6.24×10^2 or $9.36 \times 10^2 \text{ nmol}/\text{cm}^2$) at a constant Fe-TBTPP loading ($16 \text{ nmol}/\text{cm}^2$) at -0.95 V vs RHE in the CO_2 saturated 0.1 M KHCO_3 H-cell. The error bars represent the standard deviations from measurements of three independent electrodes.

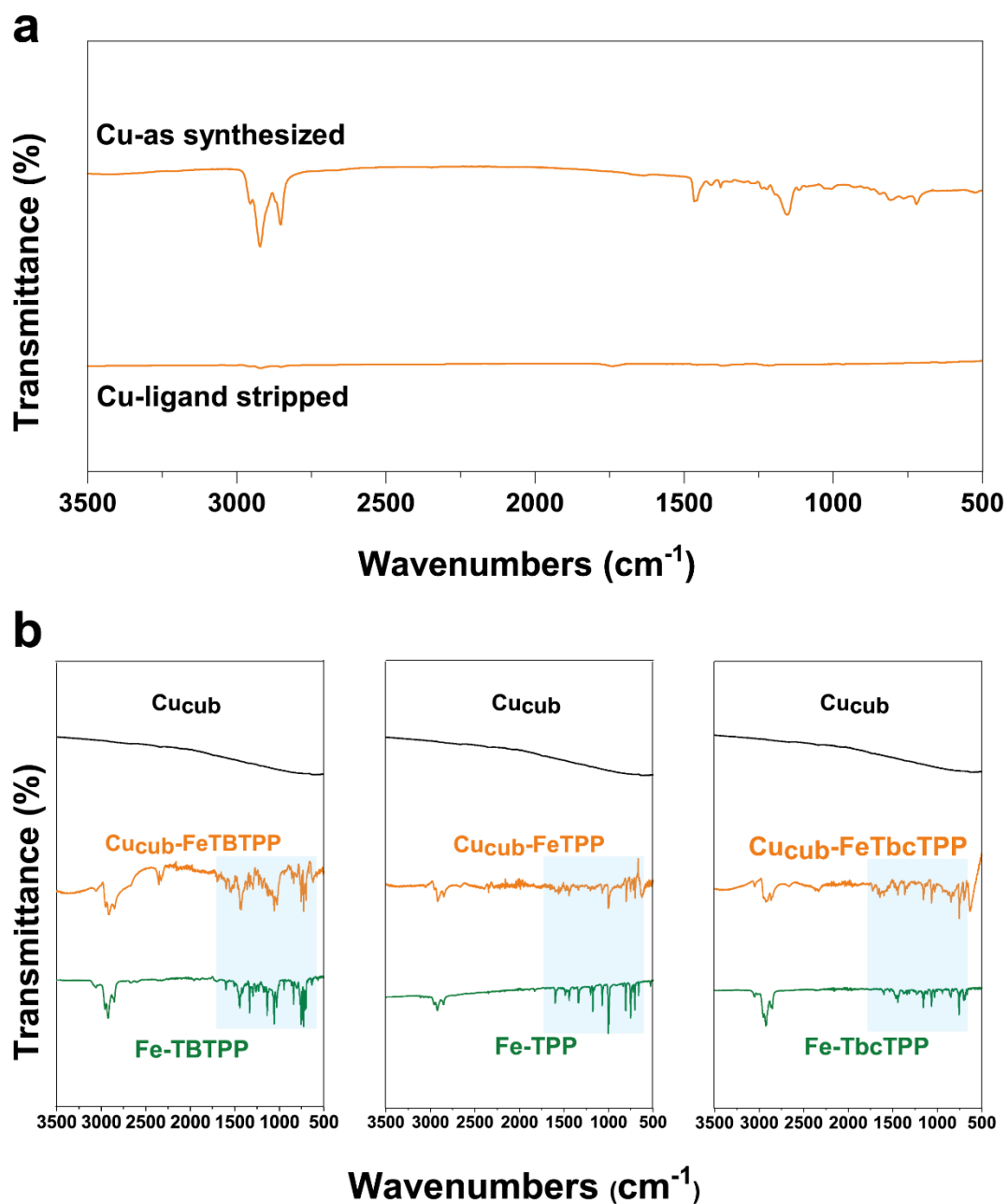


Fig. S16. (a) FT-IR of the Cu_{cub} before and after ligand stripping and (b) the pure Fe-Por and the Cu_{cub} /Fe-Por after 1.5 h electrolysis at -1.05 V vs RHE in the CO_2 saturated aqueous 0.1 M KHCO_3 H-cell. The typical peaks of Fe-Por are highlighted in blue.

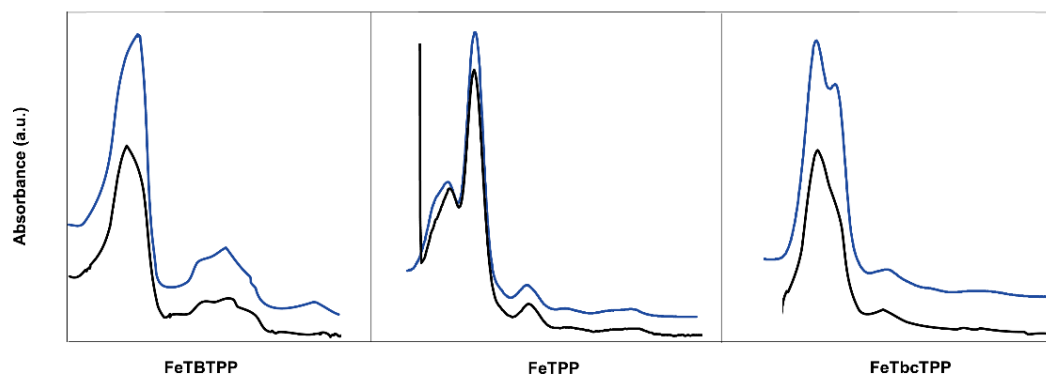


Fig. S17. UV-Vis of the as-synthesized Fe-Por (blue) and of the Fe-Por (black) after 1.5 h electrolysis at -1.05 V vs RHE in the CO₂ saturated aqueous 0.1 M KHCO₃ H-cell. The post-electrolysis Fe-Por samples were recovered from the Cu_{cub}/Fe-Por electrodes by washing with THF.

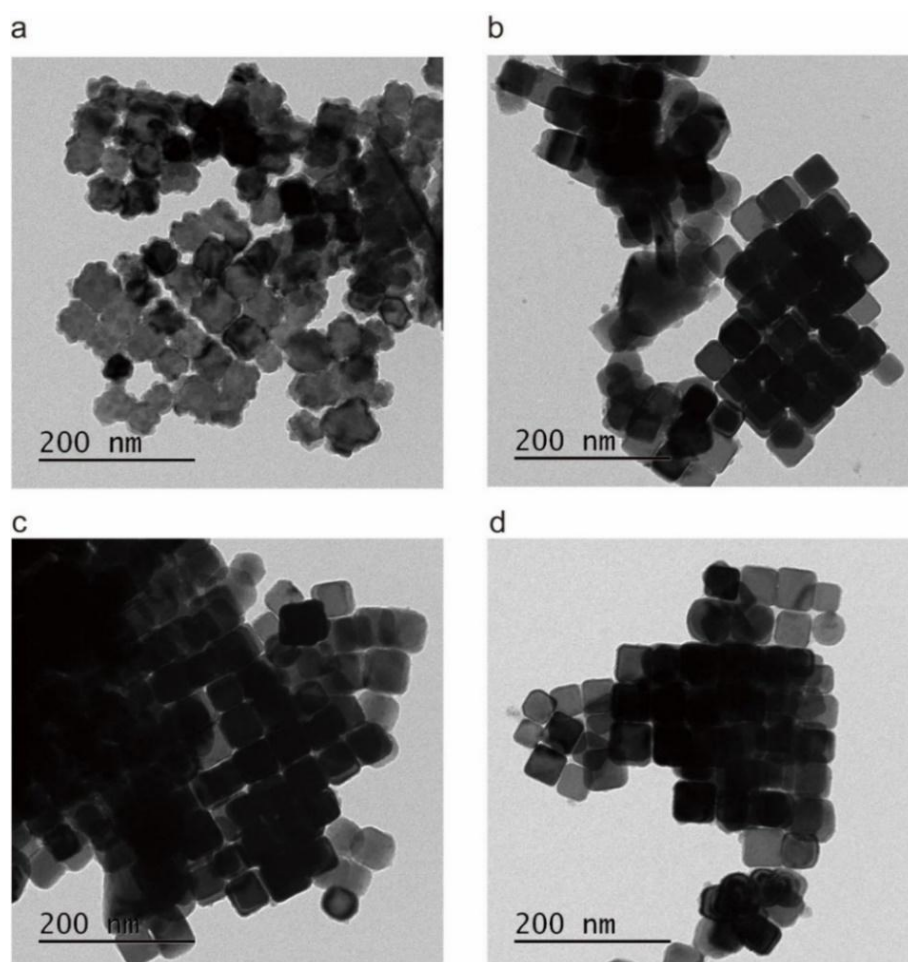


Fig. S18. TEM images of (a) Cu_{cub}, (b) Cu_{cub}/Fe-TBTPP, (c) Cu_{cub}/Fe-TPP and (d) Cu_{cub}/Fe-TbcTPP after 1.5 h electrolysis at -1.05 V vs RHE in the CO₂ saturated aqueous 0.1 M KHCO₃ H-cell.

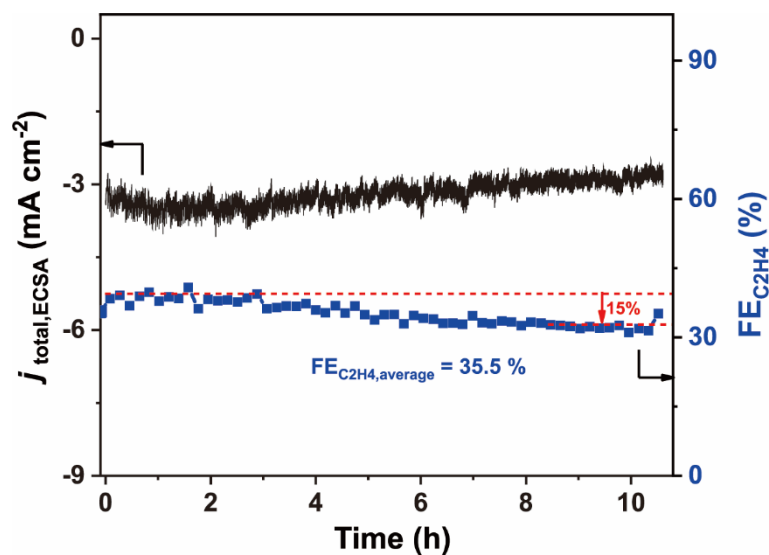


Fig. S19. Performance of $\text{Cu}_{\text{cub}}/\text{Fe-TBTPP}$ at -1.05 V vs RHE for 10 h in the H-cell using 0.1 M KHCO_3 as the electrolyte.

References

1. J. Pankhurst, P. Iyengar, V. Okatenko, R. Buonsanti, *Inorg. Chem.* 2021, **60**, 6939.
2. V. V. Pavlishchuk, A. W. Addison, *Inorganica Chim. Acta* 2000, **298** (1), 97–102.
3. I. Noviandri, K. N. Brown, D. S. Fleming, P. T. Gulyas, P. A. Lay, A. F. Masters, L. Phillips, *J. Phys. Chem. B* 1999, **103** (32), 6713–6722.
4. S. D. Jeong, B. Min, S. Y. Cho, C. Lee, B. K. Park, K. S. An, J. Lim, *The Journal of Organic Chemistry* 2012, **77**(18), 8329-8331.